17B.2 NUMERICAL SIMULATIONS OF SUPERCELLS IN CONVECTIVE BOUNDARY LAYERS

Kent H. Knopfmeier *, Paul M. Markowski, and Yvette P. Richardson
Department of Meteorology, Pennsylvania State University, University Park, PA

1. INTRODUCTION

Numerical simulations of supercell thunderstorms in horizontally homogeneous environments (e.g., Wilhelmson and Klemp 1978a, b; Weisman and Klemp 1982, 1984; McCaul and Weisman 2001) have demonstrated the importance of CAPE and wind shear in influencing storm type. With respect to supercells, numerical simulations have provided considerable insight into the dynamics of supercell rotation, maintenance, and propagation.

It is well-known that significant horizontal variability in CAPE and wind shear can exist on the meso-α and meso-β scales (e.g., Brooks et al. 1994; Markowski et al. 1998). Recent studies have explored (e.g. Kost and Richardson 2004; Kron 2004; Richardson et al. 2007) the sensitivity of simulated convective storms to meso-β-scale moisture and wind shear variations, and have found these heterogeneities can significantly influence the structure and evolution of deep, moist convection. Investigations into the influence of radiative effects on supercells (e.g., Markowski and Harrington 2005; Frame and Markowski 2008) have indicated a significant change in the low-level kinematic (i.e. vertical vorticity) and thermodynamic fields due to radiative cooling beneath the thunderstorm anvil. These alterations to the near-storm environment surrounding a supercell can significantly influence its subsequent morphology.

* *Corresponding author address:* Kent H. Knopfmeier, Department of Meteorology, Pennsylvania State University, 503 Walker Building, University Park, PA, 16803; email: khk124@psu.edu

Considerable variability on the meso-γ scale, in large part as a result of dry boundary layer convection, also has been observed (e.g., Markowski and Richardson 2007). Markowski and Richardson (2007) documented marked horizontal heterogeneity in the magnitude of the 0-1 km shear vector and of the 0-1 km storm-relative helicity within CBLs during the International H_2O Project (Weckwerth et al. 2004). However, their observational study could not address whether the meso-γ scale wind shear variability had any effect on storms.

All of these aforementioned studies suggest a need to include environmental heterogeneities in numerical simulations of convective storms. Although, as mentioned above, some prior studies have included meso-β-scale heterogeneity, even fewer numerical studies of deep, moist convection have included surface heat fluxes and convective boundary layers (e.g., Carpenter et al. 1998; this study was limited to cumulus congestus clouds, however). If desired, the computing capabilities of today now allow for high-resolution, 3D simulations of convective storms in convective boundary layers. To this end, our ongoing work explores the effects of the kinematic and thermodynamic variability of a convective boundary layer on thunderstorms. Preliminary results comparing the evolution of a supercell in a horizontally homogeneous environment to its evolution in a convective boundary layer are presented herein.

2. METHODOLOGY

2.1. Convective Boundary Layer Development

The Advanced Regional Prediction System (ARPS), version 5.2.8 (Xue et al. 1995, 2000, 2001, 2003) is employed to develop a fully convective boundary layer (CBL). The model is initialized with an analytic sounding (Fig. 1a) similar to that used by Bluestein and Weisman (2000), which contains a small capping inversion to inhibit widespread convective development. The wind profile (Fig. 1b) is characterized by 17 m s^{-1} of westerly shear over the depth of the CBL (1425 m) and 25 m s^{-1} of westerly shear in the 0-6 km layer. Surface physics are enabled with surface heat, moisture, and momentum fluxes calculated from stability-dependent surface drag coefficients. The surface skin temperature is held constant at a value of 305 K. This thermodynamic and wind shear configuration produces an environment favorable for the development of both a convective boundary layer and supercells.

Grid dimensions of 53 × 53 × 21 km^3 are employed with 200 m horizontal grid spacing and a vertically stretched grid with 75 m resolution near the surface. Periodic boundary conditions are imposed on the lateral boundaries with a rigid lid boundary condition applied to the top and bottom. A damping sponge layer is prescribed above 12 km. Random initial temperature perturbations of 0.1 K are applied within the lowest 1425 m to initiate convective motions in the domain. Within 1 hour, a well-developed CBL is formed (Fig. 2).

At this point of model integration (t = 1 hour), an ARPS restart file is created, which allows for subsequent model initialization in a horizontally inhomogeneous simulation. Also at this time, a new analytic sounding (Fig. 3a) is constructed by domain-averaging the profiles of potential temperature and water vapor mixing ratio. The domain-averaged wind profile is shown in Fig. 3b. This sounding, which is representative of the fully convective environment, can then be used for initialization in a horizontally homogeneous simulation.

2.2. Supercell in Horizontally Homogeneous Domain

To facilitate the development and evolution of a supercell, the horizontal model grid dimensions are expanded to 106 × 106 km^2. Surface physics are turned off to preclude any influence on the supercell from surface heat, moisture, and momentum fluxes. Kessler warm rain microphysics are utilized to simplify the interpretation of the model result and to prevent complications from the inclusion of ice species. Wave-radiating (open) boundary conditions are enabled on the lateral boundaries with the Durran and Klemp (1983) radiation condition applied. The relaxation coefficient is set to zero. The top and bottom boundary conditions are identical to those used in the CBL development simulation.

ARPS is initialized with the thermodynamic profile indicated in Fig. 3a, which also contains a wind profile (Fig. 3b) characterized by 20 m s^{-1} of westerly shear. A storm is initiated by a warm bubble (4 K) with a horizontal radius of 10 km and a vertical radius of 1500 m placed in the center of the domain at a height of 1500 m.

2.3. Supercell in Horizontally Inhomogeneous Domain

The model configuration in this experiment is nearly identical to the previous case, except that surface physics are once again enabled with parameters matching those used to develop the CBL, and the domain is made horizontally inhomogeneous through initialization of ARPS with the restart file mentioned in Section 2.1. To allow ingestion of this file into the model, due to their size incongruity, the restart file is expanded such that an identical copy of the initial grid is created in the x and y direction, exactly doubling the horizontal size of the domain to match the prescribed grid dimensions. The method of storm initiation in the inhomogeneous domain is identical to that utilized in the homogeneous case.

3. MODEL SIMULATION RESULTS

Time series of maximum vertical velocity, rainwater mixing ratio (qr), and low-level vorticity in the model domain are plotted for both cases in Figs. 4a-c. The vertical velocity (Fig. 4a) exhibits an initial rapid spike in both cases due to the influence of the initial warm bubble, which then levels off. Velocity comparison during the early stage of the simulation reveals that the maximum vertical velocity is higher with the supercell in the heterogeneous CBL, while during the late stages the supercell in the homogeneous CBL exhibits higher vertical velocities. However, the average maximum vertical velocity for both cases over the entire model simulation is similar. The maximum qr fields (Fig. 4b) exhibits much of the same characteristics as the velocity field, whereby the supercell in the heterogeneous CBL has a higher initial qr value and the supercell in the homogeneous CBL displays higher qr values near the end of the simulation. Still, the maximum averaged qr with time over the entire domain is nearly equal. Less variability is evident in the domain maximum vertical vorticity below 2 km (Fig. 4c). With the exception of a few small spikes in magnitude of ~ 0.05 s^{-1}, the low-level vertical vorticity in both cases is fairly similar.

Model fields from the heterogeneous CBL case (Figs. 5a-d) and the homogeneous CBL case (Figs. 6a-d) depict storm evolution at 1 h in the model simulation. Fig. 5a indicates the total vertical velocity at 1 km above mean sea level (MSL). A fairly smooth arc of ~ 10 m s^{-1} positive vertical velocity is evident signifying the leading edge of the gust front produced by the initial convective development in the center of the domain. The rainwater mixing ratio field (Fig. 5b) at 1 km above MSL shows evidence of splitting supercells with hook-like appendages on both the left- and right-movers. Vertical velocities at 5 km above MSL (Fig. 5c) of greater than 30 m s^{-1} imply intense convection with both storms, and the rainwater mixing ratio field (Fig. 5d) shows evidence of a similar hook-like feature to that at low-levels, suggesting the presence of rotation.

Model fields from the homogeneous CBL case show storm evolution similar to the heterogeneous case, with a few distinct differences. The vertical velocity field at 1 km above MSL (Fig. 6a) depicts a slightly stronger gust front, with more variability along the leading edge. In addition, the rainwater mixing ratio field at 1 km MSL (Fig. 6b), as well as the vertical velocity (Fig. 6c) and rainwater mixing ratio field (Fig. 6d) at 5 km above MSL, indicating the location of the splitting supercells, are smoother than in the heterogeneous case. Also, the rainwater mixing ratio at both vertical levels is lower in the homogeneous case.

4. FUTURE WORK

Further adjustments to the CBL development process involving ways to maintain the CBL structure over time are planned. Additional refinements to the supercell initiation experiments are expected as well.

Moreover, the effect of the supercell on the CBL itself will also be examined.

5. REFERENCES

Bluestein, H. B., and M. L. Weisman, 2000: The interaction of numerically simulated supercells initiated along lines. *Mon. Wea. Rev.*, **128**, 3128-3149.

Brooks, H. E., C. A. Doswell, and J. Cooper, 1994: On the environments of tornadic and nontornadic mesocyclones. *Wea. Forecasting*, **9**, 606-617.

Carpenter R. L., K. K. Droegemeier, and A. M. Blyth, 1998: Entrainment and detrainment in numerically simulated cumulus congestus clouds. Part I: General results. *J. Atmos. Sci.*, **55**, 3417–3432.

Durran, D. R., and J. B. Klemp, 1983: The effects of moisture on trapped mountain lee waves. *J. Atmos. Sci.*, **39**, 2490-2506.

Frame, J. W., and P. M. Markowski, 2008: Simulations of supercell thunderstorms with a radiative transfer parameterization. Preprints, *24th Conf. on Severe Local Storms*, Savannah, GA, Amer. Meteor. Soc., 17B.1.

Klemp, J. B., and R. B. Wilhelmson, 1978a: The simulation of three-dimensional convective storm dynamics. *J. Atmos. Sci.,* **35**, 1070-1096.

Klemp, J. B., and R. B. Wilhelmson, 1978b: The simulation of right- and left-moving storms produced through storm splitting. *J. Atmos. Sci.*, **35**, 1097-1110.

Kost J., and Y. P. Richardson, 2004: The influence of temporally-varying vertical wind shear on numerically simulated convective storms. Preprints, *22d Conf. on Severe Local Storms*, Hyannis, MA, Amer. Meteor. Soc., CD-ROM, 9.2.

Kron J., 2004: The evolution of numerically-modeled convection in an environment containing horizontal variations of vertical shear and low-level moisture. M.S. thesis, Dept. of Meteorology, The Pennsylvania State University, 170 pp.

Markowski, P. M., J. M. Straka, E. N. Rasmussen, and D. O. Blanchard, 1998: Variability of storm-relative helicity during VORTEX. *Mon. Wea. Rev.*, **126**, 2959-2971.

Markowski, P. M., and J. Y. Harrington, 2005: A simulation of a supercell thunderstorm with emulated radiative cooling beneath the anvil. *J. Atmos. Sci.*¸ **62**, 2607-2617.

Markowski P. M., and Y. P. Richardson, 2007: Observations of vertical wind shear heterogeneity in convective boundary layers. *Mon. Wea. Rev.*, **135**, 843–861.

McCaul. E. W., and M. L. Weisman, 2001: The sensitivity of simulated supercell structure and intensity to variation in the shapes of environmental buoyancy and shear profiles. *Mon. Wea. Rev.*, **129**, 664-687.

Richardson, Y. P., K. K. Droegemeier, and R. P. Davies-Jones, 2007: The influence of horizontal environmental variability on numerically simulated convective storms. Part I: Variations in vertical shear. *Mon. Wea. Rev.*, **135**, 3429-3455.

Weckwerth T. M., Coauthors, 2004: An overview of the International H_2O Project (IHOP) and some preliminary highlights. *Bull. Amer. Meteor. Soc.*, **85**, 253–277.

Weisman, M. L., and J. B. Klemp, 1982: The dependence of numerically-simulated convective storms on vertical wind shear and buoyancy. *Mon. Wea. Rev.*, **110**, 504-520.

Weisman, M. L., and J. B. Klemp, 1984: The structure and classification of numerically simulated convective storms in directionally varying wind shears. *Mon. Wea. Rev.*, **112**, 2479-2498.

Xue M., V. Wong, A. Shapiro, and K. Brewster, 1995: ARPS version 4.0 user’s guide. Center for Analysis and Prediction of Storms, University of Oklahoma, Norman, OK, 380 pp.

Xue M., K. K. Droegemeier, and V. Wong, 2000: The Advanced Regional Prediction System (ARPS)—A multiscale nonhydrostatic atmospheric simulation and prediction tool. Part I: Model dynamics and verification. *Meteor. Atmos. Phys.*, **75**, 161–193.

Xue M., Coauthors, 2001: The Advanced Regional Prediction System (ARPS)—A multiscale nonhydrostatic atmospheric simulation and prediction tool. Part II: Model physics and applications. *Meteor. Atmos. Phys.*, **76**, 143–165.

Xue M., D.-H. Wang, J.-D. Gao, K. Brewster, and K. K. Droegemeier, 2003: The Advanced Regional Prediction System (ARPS), storm-scale numerical weather prediction and data assimilation. *Meteor. Atmos. Phys.*, **82**, 139–170.

6. FIGURES

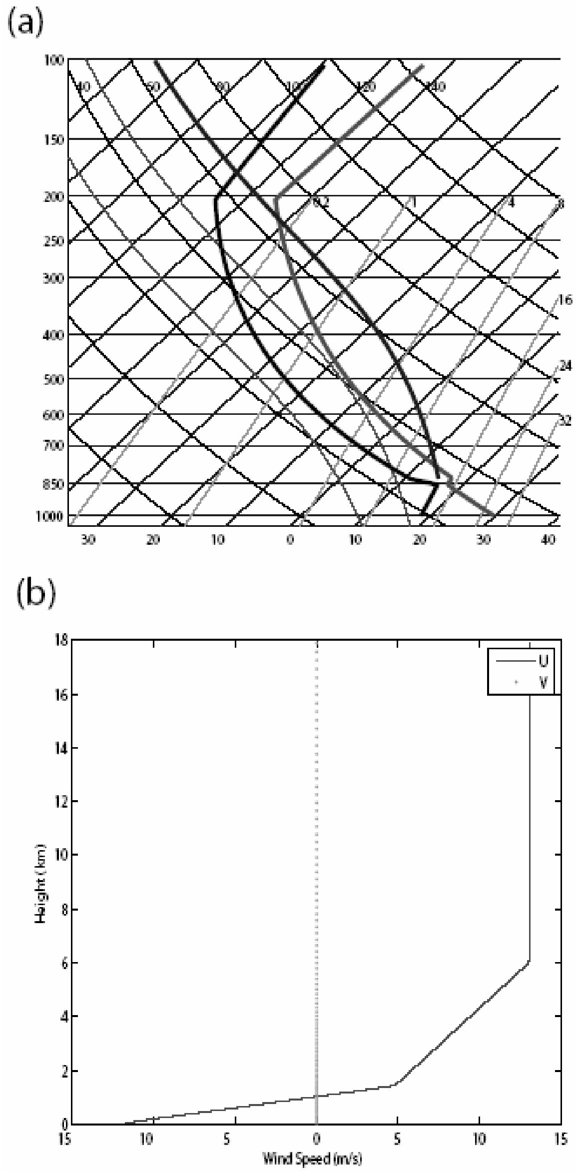

FIG. 1. (a) Skew T-log p diagram depicting the temperature and moisture profile used to initialize the CBL. (b) Wind profile used in CBL initialization.

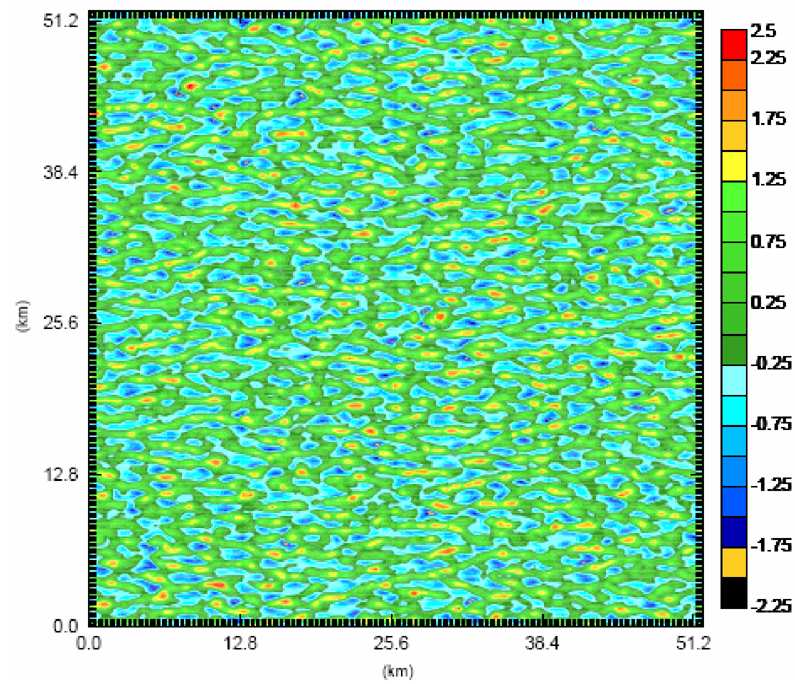

FIG. 2. Perturbation w-velocity at 500 m above mean sea level at one hour in the CBL development simulation.

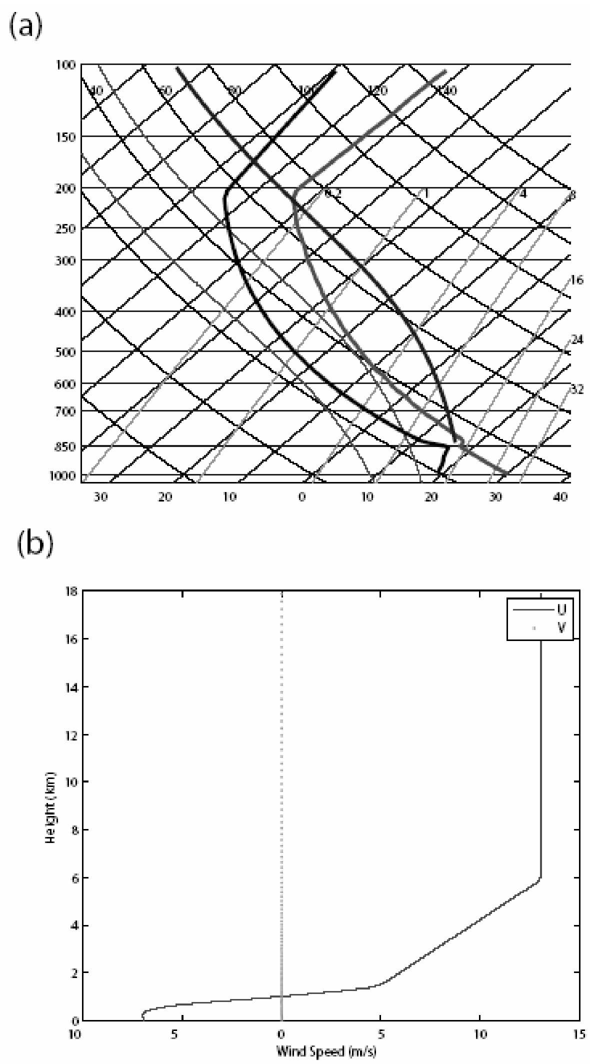

FIG. 3. (a) Skew T-log p diagram depicting the temperature and moisture profile used to initialize the supercell in a horizontally homogeneous environment. (b) Corresponding wind profile for supercell initialization.

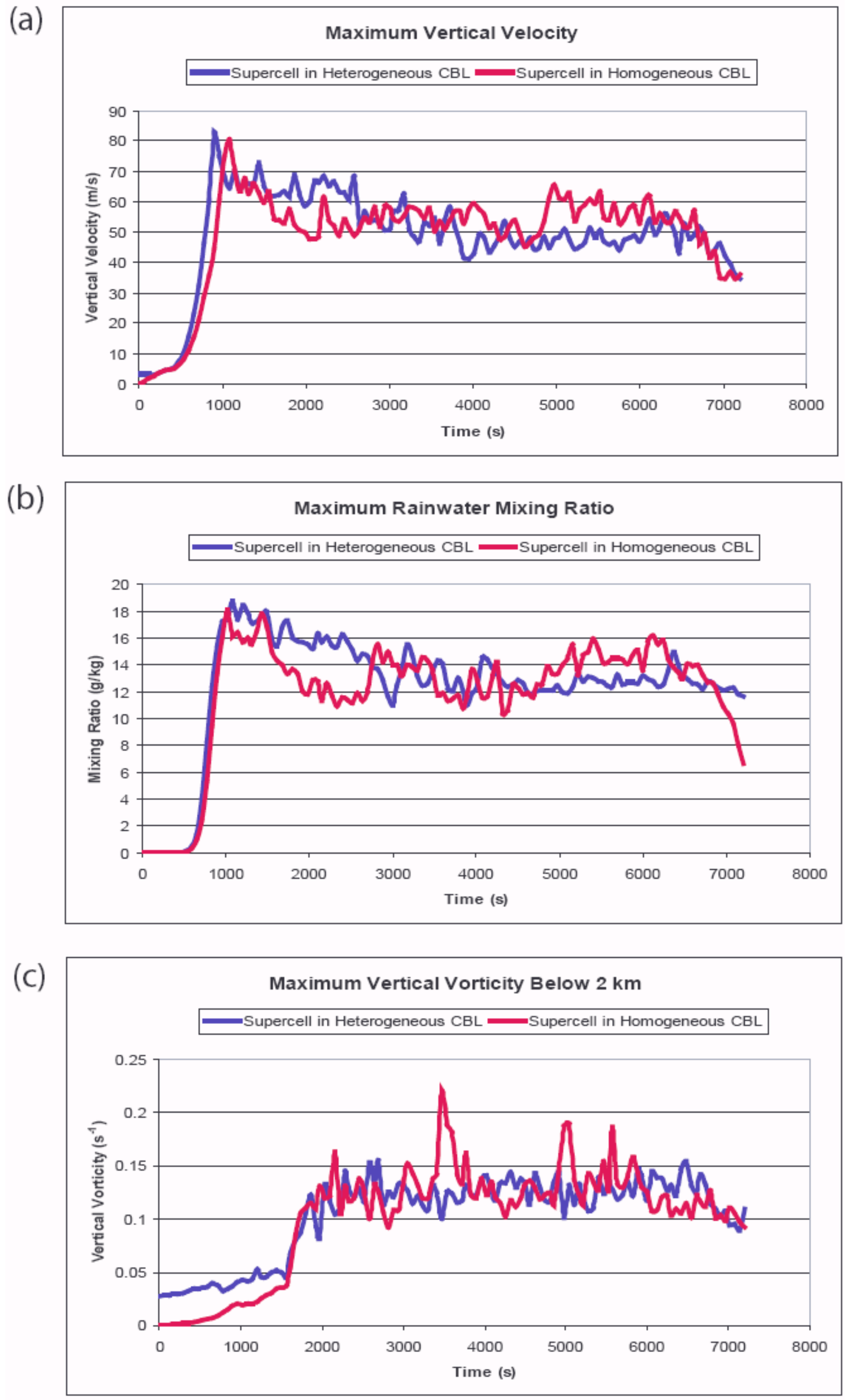

FIG. 4. (a) Maximum vertical velocity with time for a supercell in a heterogeneous CBL and a supercell in a homogeneous CBL. (b) Same as in (a), but showing maximum rainwater mixing ratio. (c) Same as in (a), but showing maximum vertical vorticity below 2 km.

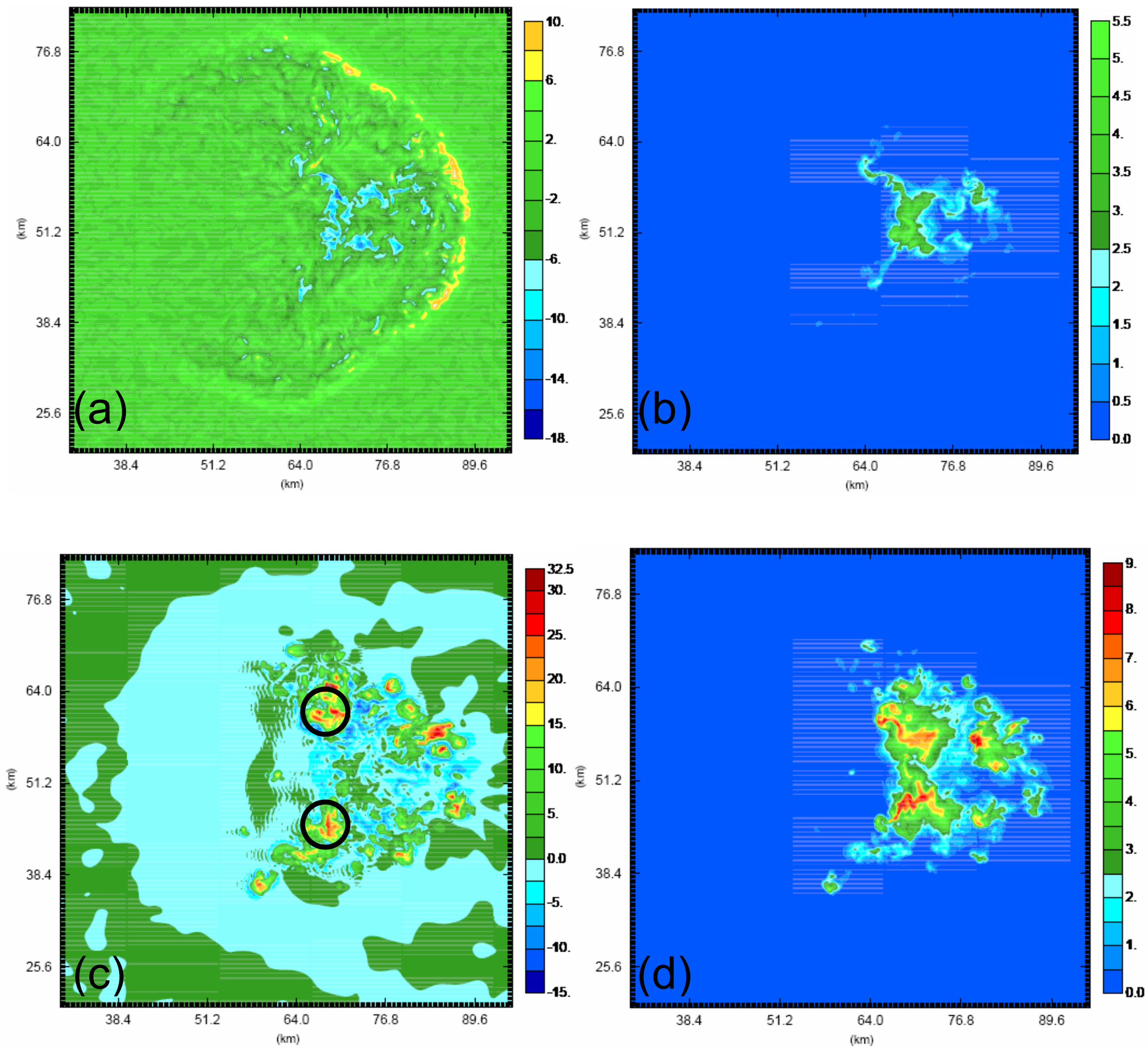

FIG. 5. (a) Vertical velocity at t = 1 h in the model simulation at 1 km above mean sea level (MSL) for the supercell in a heterogeneous convective boundary layer. (b) Same as in (a), but depicting the rainwater mixing ratio. (c) Same as in (a), but at 5 km above MSL. Black circles indicate the location of the left-moving (upper) and right-moving (lower) supercells. (d) Same as in (b), but at 5 km above MSL.

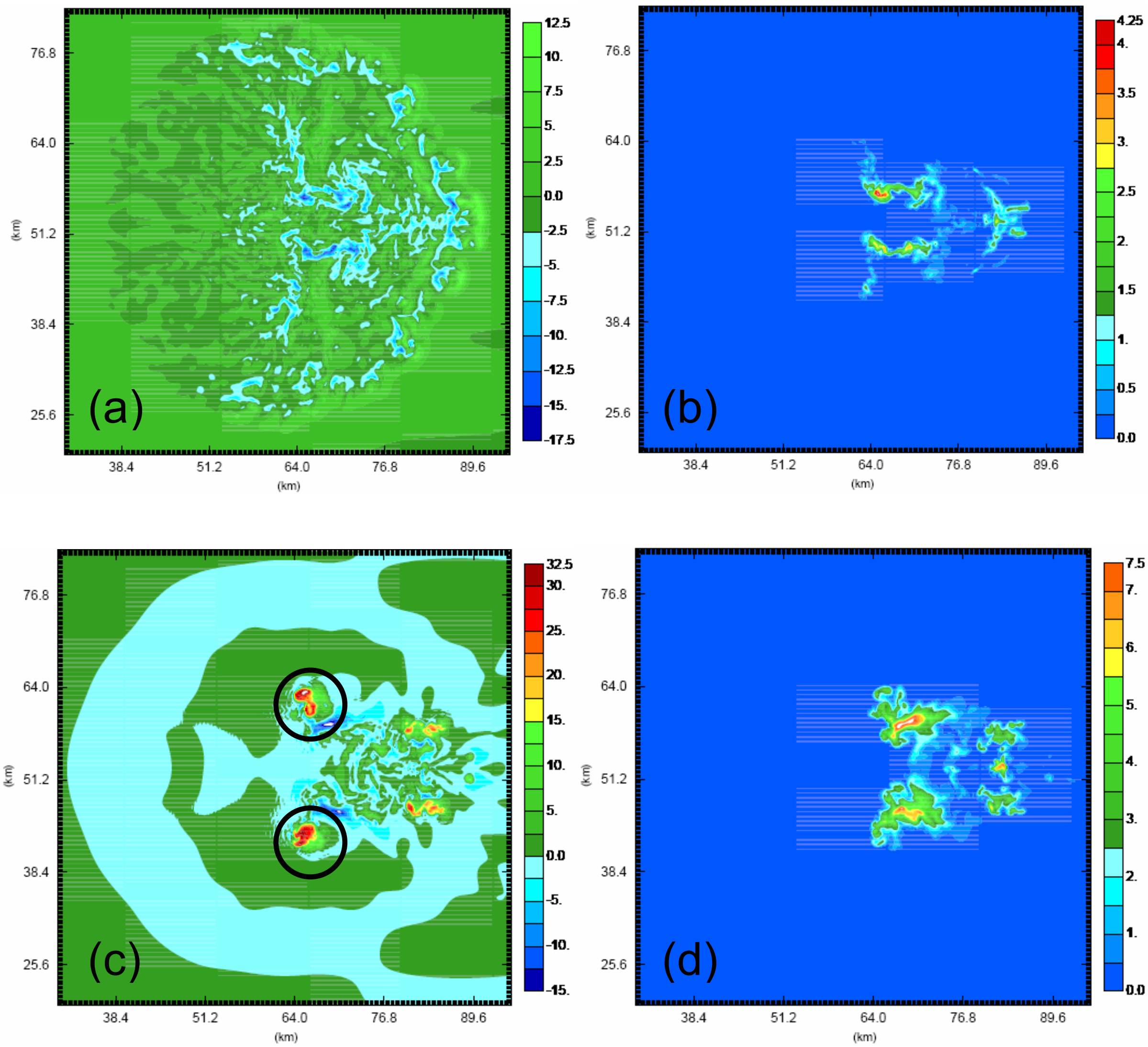

FIG. 6. (a) Vertical velocity at t = 1 h in the model simulation at 1 km above mean sea level (MSL) for the supercell in a horizontally homogeneous domain. (b) Same as in (a), but depicting the rainwater mixing ratio. (c) Same as in (a), but at 5 km above MSL. Black circles indicate the location of the left-moving (upper) and right-moving (lower) supercells. (d) Same as in (b), but at 5 km above MSL.